

Cluster Structure of ${}^9\text{Be}$ from ${}^3\text{He}+{}^9\text{Be}$ Reaction

S.M. Lukyanov¹, M.N. Harakeh², M.A. Naumenko¹, Yi Xu³,
 W.H. Trzaska⁴, V. Burjan³, V. Kroha³, J. Mrazek³, V. Glagolev³,
 Š. Piskoř³, E.I. Voskoboynik¹, S.V. Khlebnikov⁵,
 Yu.E. Penionzhkevich^{1,6}, N.K. Skobelev¹, Yu.G. Sobolev¹,
 G.P. Tyurin³, K. Kuterbekov⁷ and Yu. Tuleushev⁸

¹ Flerov Laboratory of Nuclear Reactions, Dubna, Russian Federation

² KVI-CART, University of Groningen, Groningen, Netherlands

³ Nuclear Physics Institute, Řež, Czech Republic

⁴ Department of Physics, University of Jyväskylä, Jyväskylä, Finland

⁵ Khlopin Institute, St. Petersburg, Russian Federation

⁶ National Research Nuclear University “MEPhI”, Moscow, Russian Federation

⁷ Eurasian Gumilev University, Astana, Kazakhstan

⁸ Nuclear Physics Institute, Almaty, Kazakhstan

E-mail: lukyan@nrmail.jinr.ru

Abstract. The study of inelastic scattering and multi-nucleon transfer reactions was performed by bombarding a ${}^9\text{Be}$ target with a ${}^3\text{He}$ beam at an incident energy of 30 MeV. Angular distributions for ${}^9\text{Be}({}^3\text{He}, {}^3\text{He}){}^9\text{Be}$, ${}^9\text{Be}({}^3\text{He}, {}^4\text{He}){}^8\text{Be}$, ${}^9\text{Be}({}^3\text{He}, {}^7\text{Be}){}^5\text{He}$, ${}^9\text{Be}({}^3\text{He}, {}^6\text{Li}){}^6\text{Li}$ and ${}^9\text{Be}({}^3\text{He}, {}^7\text{Li}){}^5\text{Li}$ reaction channels were measured. Cross sections for channels leading to unbound ${}^5\text{He}_{g.s.}$, ${}^5\text{Li}_{g.s.}$ and ${}^8\text{Be}$ systems were obtained from singles measurements where the relationship between the energy and the scattering angle of the observed stable ejectile is constrained by two-body kinematics. Information on the cluster structure of ${}^9\text{Be}$ was obtained from the transfer channels. It was concluded that cluster transfer is an important mechanism in the investigated nuclear reactions. In the present work an attempt was made to estimate the relative strengths of the interesting ${}^8\text{Be}+n$ and ${}^5\text{He}+\alpha$ cluster configurations in ${}^9\text{Be}$. The branching ratios have been determined confirming that the ${}^5\text{He}+\alpha$ configuration plays an important role. The configuration of ${}^9\text{Be}$ consisting of two bound helium clusters ${}^3\text{He}+{}^6\text{He}$ is significantly suppressed, whereas the two-body configurations ${}^8\text{Be}+n$ and ${}^5\text{He}+\alpha$ including unbound ${}^8\text{Be}$ and ${}^5\text{He}$ are found more probable.

1. Introduction

In recent years the study of light radioactive nuclei [1, 2] has intensified due to the significant progress made with radioactive beam facilities. It has led to a decrease of interest in the study of light stable nuclei such as ${}^6,7\text{Li}$ and ${}^9\text{Be}$. It has been shown that in light nuclei the nucleons tend to group into clusters, the relative motion of which defines to a large extent the properties of these nuclei. Consequently, the cluster structure of their ground as well as low-lying excited states became the focus of theoretical and experimental studies. For example, ${}^6\text{Li}$ and ${}^7\text{Li}$ nuclei are both well described by the two-body cluster models ($\alpha + d$ and $\alpha + t$, respectively).

Due to its Borromean structure, a special attention has been focused on the ${}^9\text{Be}$ nucleus, which could break up directly to α and a neutron, or via one of two unstable intermediate nuclei: ${}^8\text{Be}$ or ${}^5\text{He}$. The breakup of ${}^9\text{Be}$ via ${}^8\text{Be}_{g.s.}$ has been measured for many of the low-lying



excited states of ${}^9\text{Be}$ [3, 4]. However, the breakup branching via the first-excited 2^+ state of ${}^8\text{Be}$ and via ${}^5\text{He}$ remained uncertain.

In Ref. [5], the structure of ${}^9\text{Be}$ was discussed in the frame of isobaric analogue states of ${}^9\text{B}$. Charity et al. [5] found that the decay of ${}^9\text{B}$ has the dominant branch $\alpha+{}^5\text{Li}$ implying that “the corresponding mirror state in ${}^9\text{Be}$ would be expected to decay through the mirror channel $\alpha+{}^5\text{He}$, instead of through the $n+{}^8\text{Be}(2^+)$ channel. The mirror state of ${}^9\text{Be}$ at 2.429 MeV is also reported to decay by α emission”. In this case it would decay to the unstable ground state of ${}^5\text{He}$ producing the $n+2\alpha$ final state. On the contrary, another experimental work [4] claimed that this state decays almost exclusively by n emission to the unstable first-excited state of ${}^8\text{Be}$.

The excited states of ${}^9\text{Be}$ have been populated in various ways including among others β -decay [6]. Most experiments confirm that the 2.429 MeV state has a branching ratio to the ${}^8\text{Be}_{g.s.}+n$ channel of only $\sim 7\%$ [3], but could not determine whether the remaining strength was in the ${}^8\text{Be}(2^+)+n$ or the ${}^5\text{He}+\alpha$ channel. However, it was reported in Ref. [6] that the ratio 2:1 could be assigned for the two channels, respectively.

The results of Refs. [3, 4, 5] along with the qualitative breakup data discussed above suggest the necessity of obtaining quantitative branching-ratio data for the low-lying states in the Borromean nucleus ${}^9\text{Be}$.

The present experiment was designed to study the breakup of ${}^9\text{Be}$ in the attempt to determine the contribution of ${}^5\text{He}+\alpha$ and $n+{}^8\text{Be}$ channels. Our data are based on inclusive measurements, whereas the experimental results of Refs. [3, 4] were obtained in exclusive measurements. Another purpose of the present study was the attempt to find the cluster structure (for instance, ${}^5\text{He}$) and how the cluster structure influences the nuclear reaction mechanism.

The angular distributions of the ${}^9\text{Be}({}^3\text{He}, {}^7\text{Be}){}^5\text{He}$ and ${}^9\text{Be}({}^3\text{He}, {}^6\text{Li}){}^6\text{Li}$ reaction channels were scrupulously measured at the energy of 60 MeV for the transitions to the ground states of ${}^5\text{He}$ and ${}^6\text{Li}$ by Rudchik et al. [8]. The experimental data were analysed using the coupled reaction channels (CRC) model including one- and two-step cluster transfer and cluster spectroscopic amplitudes calculated in the framework of the translation-invariant shell model. It was concluded that the cluster transfer is unimportant: in the ${}^9\text{Be}({}^3\text{He}, {}^7\text{Be}){}^5\text{He}$ reaction channel the α -transfer dominates only at small angles while the transfer of two neutrons dominates at large angles. Nevertheless, the conclusion of Ref. [8] in general supports the idea of cluster transfer.

The second motivation for studying again the ${}^3\text{He}+{}^9\text{Be}$ reaction was the attempt to find evidence for the cluster structure of these nuclear systems by the analysis of the reaction products.

2. Experimental procedure

The ${}^3\text{He}+{}^9\text{Be}$ experiments were performed at the K130 Cyclotron facility of the Accelerator Laboratory of the Physics Department of Jyväskylä University and at the Nuclear Physics Institute (NPI), Řež, Czech Republic. The ${}^3\text{He}$ beam energy was 30 MeV. The average beam current during the experiments was maintained at 10 nA. The self-supporting Be target was prepared from a 99% pure thin foil of beryllium. The target thickness was 12 μm . Peaks due to carbon and oxygen contaminations were not observed in the energy spectra.

To measure (in)elastically scattered ions four Si-Si(Li) telescopes each consisting of ΔE_0 , ΔE and E_r detectors with thicknesses 10 μm , 100 μm and 3 mm, respectively, were used. Each telescope was mounted at a distance of ~ 45 cm from the target. Particle identification was based on the measurements of energy-loss ΔE and residual energy E_r (the so-called ΔE - E method). The telescopes were mounted on rotating supports, which allowed to obtain data from $\theta_{lab} = 20^\circ$ to $\theta_{lab} = 107^\circ$ in steps of 1-2 $^\circ$. The two-dimensional plots energy loss ΔE vs. residual energy E_r and ΔE_0 vs. ΔE are shown in Fig. 1a and Fig. 1b, respectively. The excellent energy resolutions of both ΔE and E_r detectors allowed unambiguous identification of A and Z of each product. The panel (a) is mainly related to the transfer from the projectile to the target,

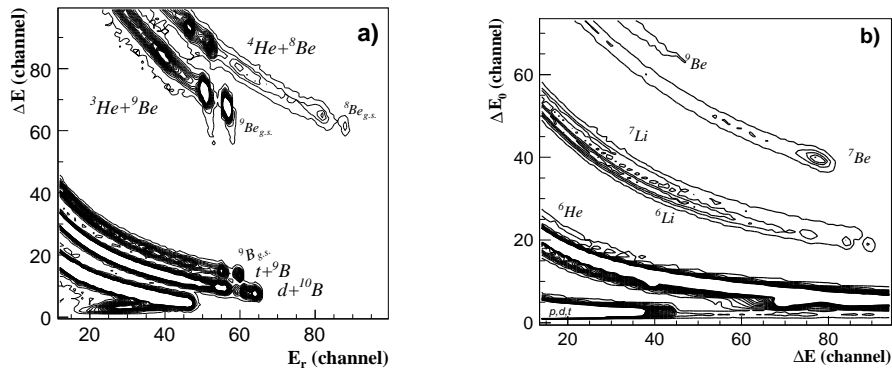


Figure 1. Particle identification plots for the products of the $^3\text{He}+^9\text{Be}$ reaction: a) p , d , t and $^3,^4\text{He}$; b) ^6He , $^6,^7\text{Li}$ and $^7,^9\text{Be}$. ΔE is the energy loss and E_r is the residual energy. The loci for the products are indicated.

whereas the panel (b) is completely related to the transfer from the target to the projectile.

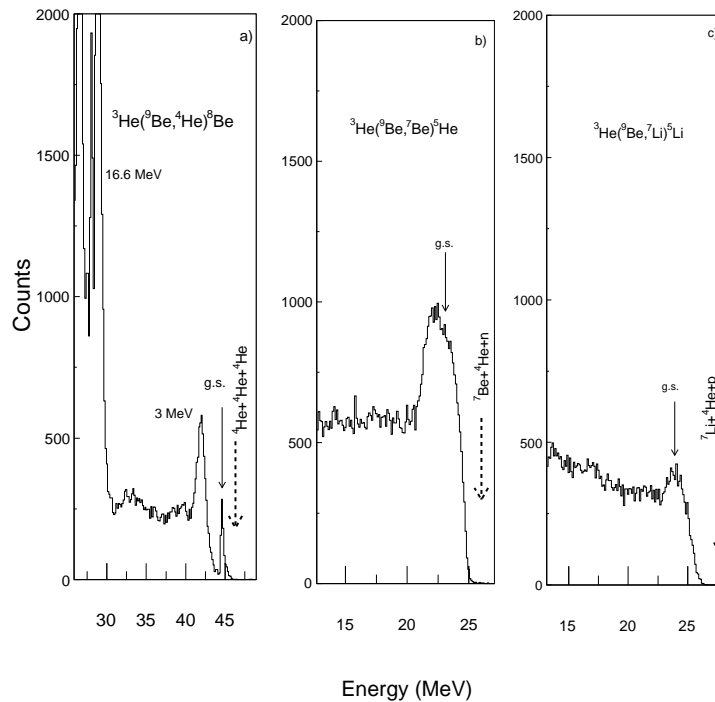


Figure 2. Spectra of the total deposited energy for the detected ^4He (a), ^7Be (b) and ^7Li (b), measured at 18° in the laboratory system for the reaction $^3\text{He}(30\text{ MeV})+^9\text{Be}$.

Fig. 2 shows experimental spectra of the total deposited energy for the detected ^4He , ^7Be and ^7Li , measured at 18° in the laboratory system for the reaction $^3\text{He}(30\text{ MeV})+^9\text{Be}$. The

plotted total energies were calculated as the sum of the calibrated energy losses ΔE s and the residual energy E_r . The ground and the most populated excited states of ${}^8\text{Be}$, ${}^5\text{He}$ and ${}^5\text{Li}$ as well as the ground states populated in the reaction channels ${}^9\text{Be}({}^3\text{He}, {}^4\text{He}){}^8\text{Be}$, ${}^9\text{Be}({}^3\text{He}, {}^7\text{Be}){}^5\text{He}$ and ${}^9\text{Be}({}^3\text{He}, {}^7\text{Li}){}^5\text{Li}$ were unambiguously identified.

Since ${}^8\text{Be}$, ${}^5\text{He}$, ${}^5\text{Li}$ and are unbound nuclei and decay into ${}^4\text{He}+{}^4\text{He}$, ${}^4\text{He}+n$ and ${}^4\text{He}+p$, respectively, we calculated the positions in the measured spectra (Fig. 2) of the maximum energies of ${}^4\text{He}$, ${}^7\text{Be}$ and ${}^7\text{Li}$, assuming either two bodies or three bodies in the exit channels. Calculations were performed with the aid of the NRV server [9]. The solid arrows show the maximum values of the kinetic energies of the detected ${}^4\text{He}$, ${}^7\text{Be}$ and ${}^7\text{Li}$, which correspond in the case of ${}^4\text{He}$, ${}^7\text{Be}$ and ${}^7\text{Li}$, to the two-body character of the reaction in the exit channels: ${}^9\text{Be}({}^3\text{He}, {}^4\text{He}){}^8\text{Be}$, ${}^9\text{Be}({}^3\text{He}, {}^7\text{Be}){}^5\text{He}$ and ${}^9\text{Be}({}^3\text{He}, {}^7\text{Li}){}^5\text{Li}$, respectively. The maximum values of the kinetic energies in the case of three-body final states in the reaction channels ${}^9\text{Be}({}^3\text{He}, {}^4\text{He}+{}^4\text{He}){}^4\text{He}$, ${}^9\text{Be}({}^3\text{He}, {}^7\text{Be}){}^4\text{He}+n$ and ${}^9\text{Be}({}^3\text{He}, {}^7\text{Li}){}^4\text{He}+p$ are shown by the dashed arrows. As can be seen from Fig. 2, the local maxima at the g.s. are close to the values corresponding to the two-body exit channels in all studied reaction channels. This indicates that the two-body reaction channels dominate leading to the unbound ${}^8\text{Be}$, ${}^5\text{He}$ and ${}^5\text{Li}$ in their ground states. Therefore, it may certainly be concluded that one-step multi-nucleon transfer is the main reaction mechanism leading to the binary exit channels.

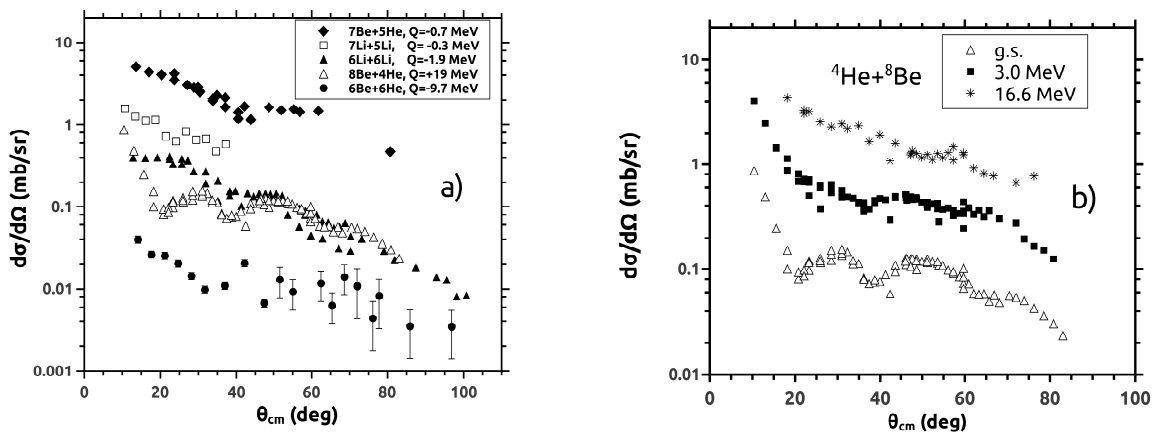


Figure 3. Angular distributions for a) ${}^3\text{He} + {}^9\text{Be} \rightarrow {}^5\text{He} + {}^7\text{Be}$ (\blacklozenge), ${}^3\text{He} + {}^9\text{Be} \rightarrow {}^5\text{Li} + {}^7\text{Li}_{g.s.}$ (\square), ${}^3\text{He} + {}^9\text{Be} \rightarrow {}^6\text{Li} + {}^6\text{Li}_{g.s.}$ (\blacktriangle), ${}^3\text{He} + {}^9\text{Be} \rightarrow {}^4\text{He} + {}^8\text{Be}_{g.s.}$ (\triangle), ${}^3\text{He} + {}^9\text{Be} \rightarrow {}^6\text{He} + {}^6\text{Be}_{g.s.}$ (\bullet); b) ${}^3\text{He} + {}^9\text{Be} \rightarrow {}^4\text{He} + {}^8\text{Be}_{g.s.}$ (\triangle), 3.0 MeV (\blacksquare) and 16.6 MeV ($*$) excited states.

3. Results

3.1. Elastic and inelastic scattering

The measured angular distributions for the reaction channels ${}^3\text{He} + {}^9\text{Be} \rightarrow {}^5\text{He} + {}^7\text{Be}$ (\blacklozenge), ${}^3\text{He} + {}^9\text{Be} \rightarrow {}^5\text{Li} + {}^7\text{Li}_{g.s.}$ (\square), ${}^3\text{He} + {}^9\text{Be} \rightarrow {}^6\text{Li} + {}^6\text{Li}_{g.s.}$ (\blacktriangle), ${}^3\text{He} + {}^9\text{Be} \rightarrow {}^4\text{He} + {}^8\text{Be}_{g.s.}$ (\triangle), ${}^3\text{He} + {}^9\text{Be} \rightarrow {}^6\text{He} + {}^6\text{Be}_{g.s.}$ (\bullet) are shown in Fig. 3a.

First of all, one may notice that the cross section for the case of ${}^5\text{He}+{}^7\text{Be}$ (\blacklozenge) is much larger than for the other reaction channels shown in Fig. 3.

The ${}^7\text{Be}$ energy spectrum (Fig. 2d) indicates the large probability of transitions to the ground state of the ${}^5\text{He}$ nucleus in conjunction with the 3^- ground state and the $1/2^-$ first-excited (0.429 MeV) state of ${}^7\text{Be}$ (unresolved in the present experiment). Therefore, the angular distribution for the ${}^5\text{He}+{}^7\text{Be}$ (\blacklozenge) channel corresponds to the ground state and the first-excited state of ${}^7\text{Be}$.

As it was mentioned, this exit channel of the reaction has the largest cross section among the channels shown in Fig. 3a. The calculated Q -values of the investigated channels are given in the inset of Fig. 3a. It may be seen that the behaviour of the cross sections does not strictly follow the famous Q -reaction systematics. For instance, the measured differential cross section for the channel ${}^4\text{He}+{}^8\text{Be}_{g.s.}$ with the maximum value of $Q = +19$ MeV is much less than for the channel ${}^5\text{He}+{}^7\text{Be}$ ($Q = -0.7$ MeV). The lowest cross section was observed for ${}^6\text{He}+{}^6\text{Be}_{g.s.}$ ($Q = -9.7$ MeV).

Fig. 3b shows the angular distributions of the differential cross sections for the ${}^3\text{He}(30\text{ MeV})+{}^9\text{Be} \rightarrow {}^4\text{He}+{}^8\text{Be}$ reaction populating the $g.s.$, and the 3.0 MeV and around 16.6 MeV excited states. It seems that the high positive Q -value of the reaction (18.9 MeV) for this channel allows to excite very high-lying levels in the unbound ${}^8\text{Be}$ nucleus. It is clearly visible from Fig. 3b that in the reaction ${}^3\text{He}+{}^9\text{Be} \rightarrow {}^4\text{He}+{}^8\text{Be}$ the cross section for 16.6 MeV level dominates over the other reaction channels.

The experimental data for ${}^9\text{Be}+{}^3\text{He}$ elastic scattering were fitted. The obtained OM potential parameters are listed in Table 1 in comparison with the parameters of Ref. [8]. The results of fitting are shown in Figs. 4 and 5 together with the experimental data.

The difference between the obtained parameters and those of Ref. [8] is probably due to the different projectile energies: our data were obtained at 30 MeV and the data of Rudchik et al. [8] were obtained at 60 MeV. For instance, the depths of the real and imaginary parts are smaller at the lower incident energy, whereas the radii are larger than in Ref. [8].

The cross section for the transfer channel ${}^9\text{Be}({}^3\text{He}, {}^4\text{He}){}^8\text{Be}_{g.s.}$ was fitted and the OM potential parameters for the exit channel ${}^4\text{He}+{}^8\text{Be}$ were obtained. In the fitting process, the OM potential parameters for the entrance channel ${}^9\text{Be}+{}^3\text{He}$ obtained in the first step were used.

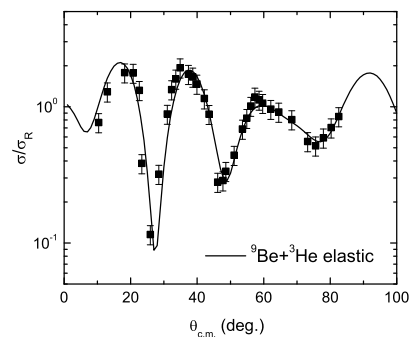


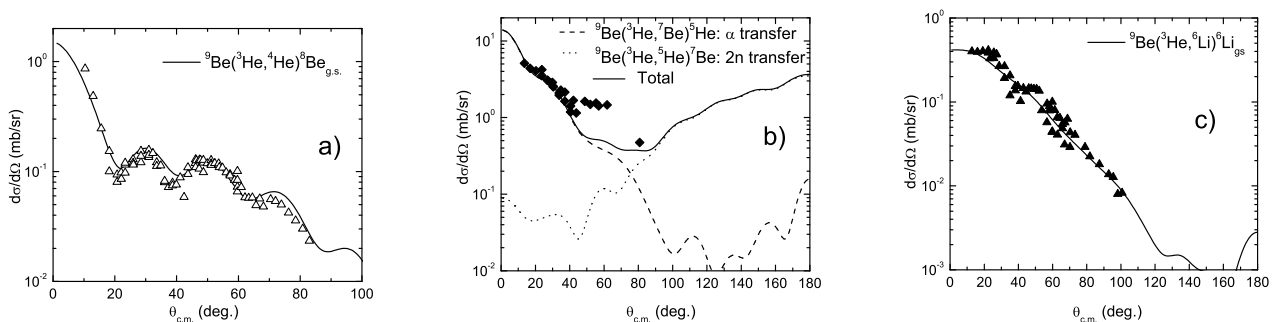
Figure 4. The ratio of the measured elastic scattering cross section to the Rutherford cross section for ${}^3\text{He}+{}^9\text{Be}$ at the incident energy 30 MeV in comparison with the OM fit.

The cross section for the transfer reactions ${}^9\text{Be}({}^3\text{He}, {}^7\text{Be}){}^5\text{He}$ was fitted simultaneously and the OM potential parameters for the exit channel ${}^5\text{He}+{}^7\text{Be}$ were obtained (Table 1). In the fitting process, the OM potential parameters for the entrance channel ${}^9\text{Be}+{}^3\text{He}$ obtained in the first step were used. In the calculations of the total cross section both transition amplitudes corresponding to the alpha-transfer mechanism (the ${}^9\text{Be}({}^3\text{He}, {}^7\text{Be}){}^5\text{He}$ channel) and the $2n$ -transfer mechanism (the ${}^9\text{Be}({}^3\text{He}, {}^5\text{He}){}^7\text{Be}$ channel) have been taken into account. All calculations and fitting have been performed using the FRESCO code [10] in the framework of the CC method.

By fitting the experimental angular distributions, the attempt was made to determine which reaction mechanisms are the most important for the measured distributions. The results are shown in Fig. 5 for the following channels: a) ${}^3\text{He} + {}^9\text{Be} \rightarrow {}^4\text{He} + {}^8\text{Be}_{g.s.}$, b) ${}^3\text{He} + {}^9\text{Be} \rightarrow {}^5\text{He} + {}^7\text{Be}$ and c) ${}^3\text{He} + {}^9\text{Be} \rightarrow {}^6\text{Li} + {}^6\text{Li}_{g.s.}$

Table 1. OM potential parameters used within the optical model and CC approaches for the reaction ${}^3\text{He}+{}^9\text{Be}$ in comparison with the parameters of Ref. [8].

| reaction channel | V_0 [MeV] | r_v [fm] | a_v [fm] | W_0 [MeV] | r_w [fm] | a_w [fm] | V_{so} [MeV] | r_{so} [fm] | a_{so} [fm] |
|-----------------------------------|----------------|---------------|---------------|----------------|---------------|---------------|-------------------|------------------|------------------|
| ${}^3\text{He}+{}^9\text{Be}$ | 108.5 | 1.123 | 0.54 | 15.69 | 1.15 | 0.855 | 13.63 | 1.83 | 0.4 |
| ${}^3\text{He}+{}^9\text{Be}$ [8] | 143.4 | 1.02 | 1.10 | 38.3 | 1.405 | 1.17 | | | |
| $\alpha+{}^8\text{Be}$ | 90.98 | 1.382 | 0.404 | 12.36 | 1.01 | 0.4 | — | — | — |
| ${}^5\text{He}+{}^7\text{Be}$ | 60.88 | 1.25 | 0.65 | 2.8 | 1.25 | 0.65 | 8.93 | 1.28 | 0.65 |
| ${}^5\text{He}+{}^7\text{Be}$ [8] | 122.5 | 0.9768 | 0.61 | 51.71 | 0.914 | 1.178 | | | |
| ${}^6\text{Li}+{}^6\text{Li}$ | 110.95 | 1.307 | 0.621 | 2.48 | 1.25 | 0.65 | 1.05 | 1.25 | 0.65 |

**Figure 5.** The angular distributions for a) ${}^3\text{He} + {}^9\text{Be} \rightarrow {}^4\text{He} + {}^8\text{Be}_{g.s.}$ (Δ), b) ${}^3\text{He} + {}^9\text{Be} \rightarrow {}^5\text{He} + {}^7\text{Be}$ (\blacklozenge) and c) ${}^3\text{He} + {}^9\text{Be} \rightarrow {}^6\text{Li} + {}^6\text{Li}_{g.s.}$ (\blacktriangle). The curves are the results of the optical-model and the coupled-channel calculations (see text).

It is clear that in the case of ${}^3\text{He}+{}^9\text{Be} \rightarrow {}^7\text{Be}+{}^5\text{He}$ reaction channel the α -transfer (long-dashed curve) dominates at forward angles, whereas the transfer of the two neutrons (short-dashed curve) dominates at backward angles.

The fit for ${}^3\text{He}+{}^9\text{Be} \rightarrow {}^6\text{Li}+{}^6\text{Li}$ (solid curve) was obtained assuming t transfer from the target nucleus to the projectile. A good agreement between the experimental data and the calculations is observed. A similar situation may be expected for the case of ${}^3\text{He}+{}^9\text{Be} \rightarrow {}^5\text{Li}+{}^7\text{Li}$ where d transfer dominates. All the values of the spectroscopic amplitudes are taken from [8].

As could be seen from Fig. 5, the main processes describing the angular distributions of the exit channels ${}^4\text{He}+{}^8\text{Be}_{g.s.}$, ${}^5\text{He}+{}^7\text{Be}$ and ${}^6\text{Li}+{}^6\text{Li}_{g.s.}$ are, respectively, the neutron, α and t transfer from the target nucleus to the projectile.

3.2. Cluster transfer in ${}^3\text{He}+{}^9\text{Be}$ reaction

Due to the Borromean structure of ${}^9\text{Be}$ the breakup of this nucleus may, in principle, proceed directly into two α particles plus a neutron or via one of the unstable intermediate nuclei: ${}^8\text{Be}$ or ${}^5\text{He}$. The attempt was made to get some insights into $n+{}^8\text{Be}$, ${}^4\text{He}+{}^5\text{He}$, $d+{}^7\text{Li}$ and $t+{}^6\text{Li}$ cluster configurations inside of ${}^9\text{Be}$ and especially to estimate the relative strengths of the most interesting ${}^8\text{Be}+n$ and ${}^5\text{He}+\alpha$ cluster configurations in ${}^9\text{Be}$.

Based on the angular distributions shown in Fig. 3, one may estimate the probability of cluster configurations in ${}^9\text{Be}$. To obtain the partition probabilities for the observed channels,

the angular distributions for each excited state (shown in Fig.3) were integrated over the solid angle. The probability was calculated as weighted integrals among the channels listed above. The obtained values of the partion probabilities are given in Table 2. The ratio of ${}^8\text{Be}+n$ to ${}^5\text{He}+\alpha$ is 2.7, which is close to the ratio 2:1 given in Ref. [6].

Table 2. Probability of cluster configurations in the ${}^9\text{Be}$ nucleus

| Exit channel | ${}^9\text{Be}$ cluster configuration | Partion probabilities (%) |
|--|---------------------------------------|---------------------------|
| ${}^4\text{He} + {}^8\text{Be}$ | $n + {}^8\text{Be}$ | $\leq 68.7 \pm 10$ |
| ${}^5\text{He} + {}^7\text{Be}$ | $\alpha + {}^5\text{He}$ | $\leq 25.1 \pm 5$ |
| ${}^6\text{Li} + {}^6\text{Li}_{g.s.}$ | $t + {}^6\text{Li}$ | $\geq 3.3 \pm 2$ |
| ${}^5\text{Li} + {}^7\text{Li}_{g.s.}$ | $d + {}^7\text{Li}$ | $\geq 2.7 \pm 2$ |
| ${}^6\text{Be} + {}^6\text{He}_{g.s.}$ | ${}^3\text{He} + {}^6\text{He}$ | $\geq 0.2 \pm 0.7$ |

Acknowledgments

We would like to thank the JYFL Accelerator Laboratory and NPI (Řež) for giving us the opportunity to perform this study as well as the cyclotron staff of both institutes for the excellent beam quality. This work was supported in part by the Russian Foundation for Basic Research (project numbers: 13-02-00533 and 14-02-91053), the CANAM (IPN ASCR) and by the grants to JINR (Dubna) from the Czech Republic, the Republic of Poland and the mobility grant from the Academy of Finland.

References

- [1] Yu E Penionzhkevich, S M Lukyanov, R A Astabatyanyan, N A Demekhina, M P Ivanov, R Kalpakchieva, A A Kulko, E R Markaryan, V A Maslov, Yu A Muzychka, R V Revenko, N K Skobelev, V I Smirnov, and Yu G Sobolev, *J. Phys. G* **36**, 025104 (2009).
- [2] N K Skobelev, N A Demekhina, R Kalpakchieva, A A Kulko, S M Lukyanov, Yu A Muzychka, Yu E Penionzhkevich, and T V Chuvilskaya, *Phys. Part. Nucl. Lett.* **6**, 208 (2009).
- [3] T A D Brown, P Papka, B R Fulton, D L Watson, S P Fox, D Groombridge, M Freer, N M Clarke, N I Ashwood, N Curtis, V Ziman, P McEwan, S Ahmed, W N Catford, D Mahboub, C N Timis, T D Baldwin, D C Weisser, *Phys. Rev. C* **76**, 054605 (2007).
- [4] P Papka, T A D Brown, B R Fulton, D L Watson, S P Fox, D Groombridge, M Freer, N M Clarke, N I Ashwood, N Curtis, V Ziman, P McEwan, S Ahmed, W N Catford, D Mahboub, C N Timis, T D Baldwin, D C Weisser, *Phys. Rev. C* **75**, 045803 (2007).
- [5] R J Charity, T D Wiser, K Mercurio, R Shane, L G Sobotka, A H Wuosmaa, A Banu, L Trache, and R E Tribble, *Phys. Rev. C* **80**, 024306 (2009).
- [6] G Nyman, R E Azuma, P G Hansen, B Jonson, P O Larsson, S Mattsson, A Richter, K Riisager, O Tengblad, K Wilhelmsen, and the ISOLDE Collaboration *et al.*, *Nucl. Phys. A* **510**, 189 (1990).
- [7] S M Lukyanov, A S Denikin, E I Voskoboynik, S V Khlebnikov, M N Harakeh, V A Maslov, Yu E Penionzhkevich, Yu G Sobolev, W H Trzaska, G P Tyurin and K A Kuterbekov, *J. Phys. G* **41**, 035103 (2014).
- [8] A T Rudchik, E I Koshhchy, A Budzanovsky, R Siudak, A Szczurek, I Skwirczynska, Yu Mashkarov, L Glowalska, J Turkiewicz, I Zalyubovsky, V Ziman, N Burtebaev, A Duyselbaev, V Adodin, *Nucl. Phys. A* **609**, 147 (1996).
- [9] V Zagrebaev, A Denikin and A Alekseev, DWBA for nucleon transfer reactions <http://nrv.jinr.ru/nrv/webnrv/transfer/> (2009), Nuclear Reaction Video Project.
- [10] I Thompson, <http://www.fresco.org.uk/>, <http://www.ianthompson.org/surrey/>.
- [11] F C Young, and A R Knudson, *Nucl. Phys. A* **184**, 563 (1972).